In-Plane Shear Behavior of Stone Masonry Panels Strengthened through Grout Injection and Fiber Reinforced Cementitious Matrices

In-plane shear behavior of stone masonry panels strengthened through grout injection and Fiber Reinforced Cementitious Matrices

Francesca Ferretti*, Andrea Incerti, Anna Rosa Tilocca and Claudio Mazzotti

Francesca Ferretti

Department of Civil, Chemical, Environmental and Materials Engineering, University of Bologna, Viale Risorgimento 2, 40136 Bologna, Italy

Phone number: +39 051 2093246, e-mail: francesca.ferretti10@unibo.it

ORCID iD: https://orcid.org/0000-0003-1484-3853

*Corresponding author

Andrea Incerti

CIRI Buildings and Construction, University of Bologna, Via del Lazzaretto 15/5, 40131 Bologna, Italy

Phone number: +39 051 2090553, e-mail: andrea.incerti3@unibo.it

ORCID iD: https://orcid.org/0000-0002-6431-3730

Anna Rosa Tilocca

CIRI Buildings and Construction, University of Bologna, Via del Lazzaretto 15/5, 40131 Bologna, Italy

Phone number: +39 051 2090513, e-mail: annarosa.tilocca@unibo.it

ORCID iD: https://orcid.org/0000-0002-4492-7890

Claudio Mazzotti

Department of Civil, Chemical, Environmental and Materials Engineering, University of Bologna, Viale Risorgimento 2, 40136 Bologna, Italy

Phone number: +39 051 2093251, e-mail: claudio.mazzotti@unibo.it

ORCID iD: http://orcid.org/0000-0002-5314-4687

In-plane shear behavior of stone masonry panels strengthened through grout injection and Fiber Reinforced Cementitious Matrices

Existing stone masonry buildings, constituting a significant portion of historical city centers, suffered often severe damages during seismic events. Traditional and innovative strengthening techniques can be applied to restore or enhance the structural capacity of these construction typologies. The objective of the present work was to evaluate the improvement given by different strengthening procedures to the shear behavior of stone masonry elements. In particular, an experimental campaign on stone masonry samples was carried out, in which the specimens were strengthened through different Fiber Reinforced Cementitious Matrix (FRCM) systems and grout injection. Non-destructive sonic tests were performed before and after the strengthening procedure to determine the efficiency of the grout injection. Then, the samples were subject to diagonal compression test with the objective of evaluating the influence of the different FRCM strengthening systems on the shear behavior, in terms of stiffness, load bearing capacity and failure mode. Comparisons between experimental results showed, on the one hand, a good correlation between the quality of the grout injection, analyzed through sonic tests, and the shear capacity of the retrofitted samples. On the other hand, the presence of the reinforcing fibers influenced mainly the post-peak behavior and determined a more ductile failure mode.

Keywords: stone masonry, diagonal compression tests, shear behavior, FRCM strengthening system, grout injection.

Introduction

The building heritage of many historical city centers, in Europe and throughout the world, is constituted by a significant number of stone masonry constructions. They are characterized by a great variability in terms of structural typology since they were built from ancient times using different construction techniques and materials (Binda et al. 2005; Penna 2015). Most of these buildings were not designed to withstand horizontal actions. Therefore, during the last decades, several seismic phenomena have shown the high vulnerability of existing stone masonry buildings, which experienced both out-of-

plane and in-plane failures (Augusti, Ciampoli, and Giovenale 2001; D'Ayala and Speranza 2003; Indirli et al. 2013). In particular, significant damages were registered for buildings in which the stone masonry piers were characterized by multiple wall leaves not effectively connected with transversal elements or, more in general, by the presence of large voids or incoherent materials (e.g. rubble infills) within the wall thickness (Ceci et al. 2010). The historical and cultural value of these construction typologies makes it necessary to preserve them through the application of appropriate strengthening procedures, aimed at ensuring both aesthetic and structural performances to the masonry elements. With the objective of improving the seismic behavior of existing stone masonry buildings, by repairing damaged structural elements or by strengthening undamaged ones, different retrofitting procedures, both traditional and innovative, could be adopted.

Concerning traditional techniques, a particular focus is here devoted to the execution of grout injection, which was proven to be suitable in providing a more homogeneous behavior to the masonry walls, by filling the voids and the cracks and improving the connections between the wall leaves (Miltiadou-fezans et al. 2006; Vintzileou et al. 2015). An adequate mortar mix for the grout should be designed to ensure its compatibility with the masonry substrate and an efficient filling ability of the voids within the wall. Moreover, to guarantee the effectiveness of the interventions without determining wall disruptions, the injection pressure has to be maintained sufficiently low (Binda et al. 2005).

Many researches were carried out to analyze the most appropriate mix designs for the grout (Vintzileou 2007; Luso and Lourenço 2016), and to develop experimental procedures capable of evaluating their efficiency. Non-destructive tests, such as sonic tests, were mainly used for this purpose (Binda 1995; Binda et al. 1997; Schuller et al. 1997; Binda, Saisi and Tiraboschi 2001; Jorne, Henriques and Baltazar 2014). Indeed, if

performed before and after the injection, the sonic tests were successful in detecting the effectiveness of the repair technique. In particular, they can generally provide qualitative information about the masonry under investigation and they can allow the control of the distribution of the grout in the masonry. Attempts to correlate the results of sonic tests with the mechanical properties of stone masonry were made (Binda, Saisi and Tiraboschi 2000; Valluzzi et al. 2018). In some cases, destructive tests were also performed to evaluate the improvement given by the grout injection to the shear behavior of stone masonry elements (Miltiadou-fezans et al. 2006; Miranda, Milosevic and Bento 2017; Silva et al. 2014).

Concerning innovative strengthening techniques, in the last years, the research has been mainly concentrated on the use of fiber reinforced composite materials, such as Fiber Reinforced Polymers (FRP) and Fiber Reinforced Cementitious Matrix (FRCM). When dealing with masonry elements, the use of FRCM systems instead of FRP is preferable due to the greater compatibility of the inorganic matrix with the masonry substrate (Papanicolaou, Triantafillou and Lekka 2011). FRCMs are also characterized by a good permeability and a good behavior at high temperatures. Several researches were focused on the mechanical characterization of FRCM, mainly through direct tensile tests and bond tests (de Felice et al. 2016; Caggegi et al. 2017; Carozzi et al. 2017; Leone et al. 2017; Lignola et al. 2017; de Felice et al. 2018; Bellini, Bovo and Mazzotti 2019; Belluni, Shahreza and Mazzotti 2019). Many combinations of mortar matrix and fibers were studied, including the use of cement- and lime-based mortars and different fiber typologies. Indeed, unidirectional fiber strips or bidirectional fiber grids, made of different materials (e.g. carbon, glass, steel, basalt, aramid, etc.) can be adopted. The FRCM application on different masonry substrates, such as brick masonry, tuff masonry and stone masonry, was investigated (Parisi et al. 2013; Feo et al. 2016; Incerti et al. 2017;

Incerti, Ferretti and Mazzotti, 2019) and some studies were also conducted to compare the performances of masonry samples strengthened by FRCM and FRP (Ferretti et al. 2015, 2016).

With the aim of evaluating the efficiency of FRCM strengthening systems in enhancing the in-plane shear capacity of masonry panels, various researches were carried out, in which the behavior of samples strengthened with different materials and layouts was compared (Faella et al. 2010; Babaeidarabad, De Caso and Nanni 2014; Ferretti et al. 2017; Incerti et al. 2019). In general, the performances of masonry elements were significantly improved by the use of these innovative strengthening systems, both in terms of shear capacity and ductility. The cited researches were mainly devoted to the study of brick masonry, while very few can be found concerning the structural strengthening of stone masonry elements (Feo, Luciano and Misseri 2016; Gattesco, Amadio and Bedon 2015; Guerreiro et al. 2018).

In the present paper, an experimental campaign was carried out with the primary objective of studying the in-plane shear behavior of rubble stone masonry panels strengthened by means of FRCM. The strengthening systems were applied on masonry specimens, built with the aim of reproducing a typical arrangement of ancient Italian existing rubble stone masonry structural elements, usually characterized by the use of poor-quality lime-based mortars, strongly irregular stones and by the presence of significant voids within the wall thickness. The study and the analysis of the most appropriate and efficient strengthening procedures is essential for this masonry typology, which typically shows weak performances in the event of an earthquake. Grout injection was also performed on the specimens and different strengthening systems were applied, having different characteristics both in terms of materials and layouts. Sonic tests were executed to evaluate the masonry quality before and after the retrofitting procedure. The

samples were, then, subject to diagonal compression tests to evaluate the efficiency of the different strengthening solutions adopted. Correlations between the results of the tests are presented in the following. The use of the digital image correlation (DIC) technique allowed to better capture the cracking development and propagation during the tests.

Experimental program

In the present experimental campaign, seven stone masonry panels were built by using rubble sandstones and natural hydraulic lime-based mortar. In more details, a unique continuous masonry wall, with dimensions 7700x1100x300 mm^3, was initially built and cured in laboratory conditions (Figure 1). The masonry pattern was arranged with two outer leaves and a chaotic internal filling, containing smaller stones and mortar and characterized by an average thickness of approximately 80 mm, depending on the dimensions of the stones. After 28 days of aging, the wall was cut to obtain seven square samples, having dimensions of 1100x1100x300 mm^3.

One unreinforced sample was used to provide for the reference behavior, while six panels were grout injected to fill the internal voids and improve the monolithic behavior of the specimens. This is a procedure typically adopted in-situ for the retrofitting of existing stone masonry structures. Among the injected samples, two panels were strengthened through grout injection only while four others were also strengthened by means of different FRCM systems: in more details, they were applied on both lateral surfaces of the samples (*SL* – symmetric layout) or on one side only (*AL* – asymmetric layout), using a continuous reinforcement (*C*) or a discontinuous one (*D*) according to configurations described in Table 1 and shown in Figure 2.

Continuous and symmetric strengthening layouts were characterized by the use of bidirectional basalt grids (B200 and B400), while the discontinuous strengthening was

obtained by using 150 mm wide unidirectional steel fiber (S600) strips. The asymmetric layout was characterized, on one side, by the application of a bidirectional basalt grid (B200), and, on the other side, by a reinforced structural repointing, executed according to the *Reticolatus* technique (Borri, Castori and Corradi 2011), using unidirectional steel fibers positioned inside the mortar joints. This technique can be adopted when there is the need of maintaining the stone masonry texture visible, e.g. in historical buildings. The characteristics of the tested samples are summarized in Table 1, while the detailed descriptions of the strengthening procedure and the testing program are presented in the following Sections.

The choice about the strengthening systems investigated in the present experimental campaign was based considering some of the most diffused strengthening layouts, typically adopted in interventions on existing stone masonry panels. They were designed according to the state of the art about FRCM applications and following the indications reported in the Italian CNR Guidelines (CNR-DT 215/2018). With the aim of studying and comparing the efficiency of different FRCM strengthening systems, two different basalt bidirectional grids were chosen (B200 and B400), characterized by different density. Moreover, a discontinuous system was also considered, since it represents a strengthening solution encountered in various real applications. Its layout was defined considering the strip width and spacing usually adopted in practice together with the geometry of the sample, characterized by limited dimensions. The asymmetric layout was chosen to reproduce the condition in which it is not possible to apply the FRCM reinforcements on both sides of a masonry wall. This is the case of many historical buildings, where the stone texture should remain visible due to esthetical and conservative reasons. The overall thickness of the adopted FRCM systems was equal to 8 mm per side, independently from the adopted grids or strips.

The FRCM strengthening systems analyzed in the present experimental campaign do not represent an upper limit regarding the amount of fibers that could be applied on stone masonry samples. Textiles with different properties and multiple layer of reinforcement could also be adopted. However, it could be difficult to state that a strength increase or a different behavior could be expected by simply increasing the amount of fibers. The complex interaction between the geometry, the stiffness, the strength of the textile and the characteristics of the matrix should be considered and studied by performing tensile and bond tests for the mechanical characterization of the systems. Indeed, when designing FRCMs, the bond behavior is crucial and can limit the efficiency of the textile.

Concerning advantages and disadvantages of the adopted FRCM systems, it can be stated that a continuous layout could be more effective than a discontinuous one since it provides a diffuse reinforcement over the masonry wall. However, a discontinuous layout could also be an adequate strengthening solution, since the unidirectional fibers can be applied along the most convenient directions, according to the stress state acting on the structural elements. Asymmetric strengthening layouts are the less effective and they should be adopted only when the intervention on both sides of the masonry wall is prevented.

Strengthening procedure

The strengthening procedure adopted in the experimental campaign for samples with symmetric FRCM arrangement consisted in the following steps (Figure 3): (i) drilling of 4 holes with 20 mm diameter, used later both for the positioning of the mechanical anchorages and for the grout injection; (ii) regularization of the two surfaces of the samples until reaching an even surface and application of the first mortar matrix layer, the latter having a thickness of 4 mm. It was applied with an offset of 20 mm from the

lateral edges of the specimens to prevent early debonding phenomena (Incerti et al. 2015). In case of discontinuous reinforcement, the mortar was applied along the reinforcing strips only; (iii) application of the unidirectional steel fiber strips or bidirectional basalt grids; (iv) positioning of the mechanical anchorages, consisting of unidirectional steel fibers bundles and a glass reinforced polypropylene dowel; (v) application of the second mortar matrix layer, with a thickness of 4 mm; (vi) sealing of the voids on the lateral surfaces of the samples by means of lime-based mortar; (vii) execution of grout injection. They were performed trough the existing holes, starting from the bottom of the samples and controlling the pressure of the mortar while injecting by means of a pressure gauge. The procedure was stopped when a significant increase in the pressure occurred.

For the stone masonry panel strengthened with an asymmetric layout, the reported procedure is still valid, except for the fact that the continuous bidirectional grid was applied only on one side of the sample. On the other side, steel fibers cords (S600), anchored inside the drilled holes, were spread along the mortar joints according to the structural repointing scheme (*Reticolatus*), as shown in Figure 4.

Concerning the samples strengthened by means of grout injection only, the role of the mechanical anchorages was also studied with the objective of evaluating their contribution to the shear capacity of the samples, since they could improve the transversal connection of the wall leaves leading to a monolithic behavior. To this purpose, mechanical anchorages were not adopted on the sample S_I, while they were used on the sample S_I-MA. For these wall panels, the strengthening procedure previously described was adapted accordingly.

Testing program

The testing program of the experimental campaign was articulated in two different phases, in which non-destructive and destructive tests were performed sequentially. More

in detail, in the first phase, non-destructive sonic tests were conducted on each sample to evaluate the quality of the plain masonry before the grout injection and the reinforcement application. Then, after the strengthening procedure, sonic tests were performed again to evaluate the improvement given by grout injection and FRCMs. In the second phase, standard diagonal compression tests were executed on the stone masonry samples to evaluate the efficiency of the strengthening system adopted in terms of load bearing capacity and failure mode. Correlations between the results of sonic tests and diagonal compression tests were carried out to better understand the shear behavior observed during the destructive tests, especially considering the cracking development and propagation.

Materials and methods

Stones

The stone elements used in the experimental campaign were natural sandstones of variable dimensions. For their mechanical characterization, 5 cubic specimens (100x100x100 mm^3) were cut and tested in compression. The mean compressive strength was equal to 38.9 MPa (CoV = 34.7%).

Mortars

In the experimental campaign, three different pre-mixed natural hydraulic lime-based mortars (NHL) were adopted: one for the construction of the stone masonry walls (NHL1), one for the grout injection (NHL2) and one used both for the regularization of the surfaces of the samples and as a matrix in the FRCM strengthening systems (NHL3). NHL2 and NHL3 mortars were both characterized by a good compatibility with the stone masonry substrate. Standard laboratory tests were conducted to evaluate their mechanical

properties (EN 1015-11), reported in Table 2. In particular, monotonic and cyclic uniaxial compression tests were performed to determine the mortar compressive strength $f_{m,c}$ and the elastic modulus E_m, respectively, while three-points bending tests were conducted to evaluate the mortar flexural strength $f_{m,fl}$.

Reinforcing fiber strips and grids

The strengthening systems chosen to retrofit the stone masonry samples were composed by unidirectional steel fiber strips or bidirectional basalt grids, arranged according to different layouts. More in details, two different basalt grids were adopted: one (B400) having a fiber amount doubled with respect to the other (B200).

Direct tensile tests were performed on three FRCM specimens per reinforcing typology to characterize the systems in terms of fiber tensile strength $f_{f,t}$, ultimate strain ε_u, elastic modulus E_f. The specimen dimensions were equal to 400x40x10 mm^3 for the basalt FRCMs and to 500x50x6 mm^3 for the steel reinforcements. The results are reported in Table 3, together with the density, the bundle spacing and the equivalent thickness t_{Vf} of the reinforcing fibers. With reference to the fiber elastic modulus, it was calculated according to standard procedures (Carozzi et al. 2017; Leone et al. 2017) by considering the final branch of the constitutive law, in which the matrix was fully cracked.

For a complete mechanical characterization of the FRCM composites, the results of single-lap shear tests, performed in a different experimental campaign (Santandrea et al. 2016), were also considered. The three investigated FRCM systems were applied on one side of brick masonry prisms, composed by 7 courses and having dimensions of 120x120x445 mm^3. For all the systems, the bonded length, the bonded width and the thickness of the FRCM composites were equal to 345 mm, 50 mm and 8 mm, respectively. The test setup is described in detail in the cited research (Santandrea et al.

2016). The obtained bond strength $f_{f,b}$, calculated considering the fibers cross section, is reported in Table 3 for each FRCM system. For bidirectional basalt grids with a low density (B200), the failure mode was characterized by the fiber rupture, while the prevalent failure mode for both bidirectional basalt grid with a high density (B400) and steel unidirectional fiber strips consisted in a delamination at the fiber-matrix interface. The single-lap shear tests, conducted on brick masonry specimens, can be considered representative also for the case of FRCM systems applied to stone masonry, since the substrate was never involved in the failure process.

Sonic tests

Sonic test is a non-destructive technique usually adopted for the diagnosis of existing masonry buildings, allowing for the evaluation of material homogeneity and the identification of possible weaknesses inside the structural elements, such as voids and cracks. According to the direct arrangement of the test, chosen in the present experimental campaign, the sonic waves are generated by an instrumented hammer (emitting probe) that produces an instantaneous impact on the surface of the specimen. On the other side of the wall panel, a sensor (receiving probe) receives the signal. The time of flight, i.e. the time taken by the waves to travel through the thickness of the masonry wall, is measured to calculate the wave velocity, which is the main outcome of a sonic test and can give information about the material quality. Indeed, the wave velocity is influenced by the physical and mechanical properties of the material through which the wave travels.

In this work, direct sonic tests were performed on each specimen, before the application of the reinforcements (plain masonry) and after the strengthening procedure. The objective was mainly to evaluate the masonry quality, heterogeneity and the effectiveness of the grout injection. In particular, a 800x800 mm^2 grid was defined over

the lateral surface of the masonry walls, having a grid spacing of 200x200 mm^2 (Figure 5*a*). At each node of this grid, three sonic tests were performed, and the average wave velocity was calculated. Wave velocity contour plots were then created by means of a spline nonlinear interpolation of the results obtained in each point of the grid. The instrumentation used for the sonic tests, constituted by two sensors (emitting and receiver) and by the control unit for data acquisition, is shown in Figure 5*b*.

Digital Image Correlation

The Digital Image Correlation (DIC) technique was used to evaluate displacements and strains evolutions over the entire lateral surface of the stone masonry samples during the diagonal compression tests. For the application of the DIC technique, one side of each stone masonry panel was prepared by painting the surface with a white paint and, subsequently, creating a random speckle pattern with black dots, realized by appropriate size marker. To achieve maximum accuracy and avoiding high noise level, the dimensions of the black dots was equal to 4x3 pixels in size, corresponding to 3.56x2.58 mm^2 in real dimensions. To obtain 3D full-field maps of strains and displacements, a stereoscopic system was used, constituted by two high resolution digital cameras (2452x2056 pixels per photogram) with a focal length equal to 35 mm, positioned with a 900 mm distance and 20° angle between them.

Diagonal compression tests

Diagonal compression tests were performed, according to the ASTM E519 and RILEM-LUMB6 Standards, to evaluate the shear capacity of the seven stone masonry samples. Tests were carried out under displacement control to better capture the post-peak behavior, according to the setup shown in Figure 6. Steel cradles allowed the specimens to be seated properly. The servo-hydraulic system used for the application of the diagonal

compression load was characterized by a maximum capacity of 500 kN. The imposed displacement rate was equal to 0.008 mm/s. Linear potentiometers, characterized by a 50 mm stroke and a 1100 mm gage length, were positioned along the diagonals of the samples, on both sides. Moreover, as already explained, the panels were accurately prepared on one side for the application of the DIC technique.

The state of stress in the center of the wall panel during a diagonal compression test is a combined stress state, which can be calculated, according to an elastic solution (Frocht 1931; Yokel and Fattal 1976; Calderini, Cattari and Lagomarsino 2010), as:

$$\sigma = 0.56\frac{P}{A_n} \tag{1}$$

$$\tau = 1.05\frac{P}{A_n}, \tag{2}$$

where σ and τ are the compressive and shear stresses, respectively, P is the applied diagonal load and A_n is the cross section of the sample. At failure, the values of the principal stresses (σ_I and σ_{II}), acting along directions which coincide with the two diagonals of the panel, are equal to:

$$\sigma_I = f_t = 0.5\frac{P_f}{A_n} \tag{3}$$

$$\sigma_{II} = 1.62\frac{P_f}{A_n}, \tag{4}$$

where f_t is the masonry diagonal tensile strength, and P_f is the failure load.

During the test, elongations and shortenings were measured along the two diagonals. Therefore, the shear strain γ can be evaluated as:

$$\gamma = \varepsilon_c + \varepsilon_t, \tag{5}$$

where ε_c and ε_t are the compression and the tensile diagonal deformations, respectively, calculated as the average between the correspondent deformations on the two sides of the

specimen.

The shear modulus G of the masonry panel was evaluated considering the tangential stress τ *vs* shear strain γ diagram. In this work, the secant modulus between 1/10 and 1/3 of the failure load was considered.

Experimental results

The results of the experimental campaign are presented in this section, starting from sonic tests and proceeding with diagonal compression tests, separately. A comparison is then discussed with the aim of better interpreting the results of the destructive tests and of correlating the outcomes of the different tests performed.

Sonic test results

The sonic test results are presented in Figure 7 in terms of average sonic wave velocity for the single masonry panels, before and after the strengthening procedure. The average values were determined by considering the results of all the sonic tests performed on each specimen. It can be noticed that unreinforced stone masonry samples were characterized by average sonic wave velocities in the range of 1168÷1464 m/s. The lowest values were registered for the samples S_URM and S_I-MA_B200-S600, probably because they were both located at the extremities of the unique stone masonry wall, and, therefore, some differences with respect to the other samples, due to the construction process, could be expected.

Strengthened samples showed higher values of average sonic wave velocities, in the range of 1418÷1933 m/s. A quite significant increment was registered, equal to 30% on average, proving the beneficial effect of the strengthening procedures to the overall quality of the stone masonry samples. This increment can ideally be associated to the presence of both the grout injection and the FRCM systems. However, it is believed that

the contribution given by the injection is much greater, because they allow to fill the internal voids of the samples, providing a better connection between the external wall leaves and improving the masonry homogeneity within the wall thickness. In particular, the most significant improvement was registered for the sample S_I-MA_S600, followed by the sample S_I. This confirms the effectiveness of injection alone, given that these wall panels were not characterized by the application of continuous FRCM systems over the lateral surfaces.

To better analyze the results of the sonic tests, sonic wave velocity maps are presented in Figure 8, Figure 9 and Figure 10 for three samples, before and after the strengthening procedure. In particular, these samples, S_I-MA_S600, S_I and S_I-MA_B400, are representative of the maximum, an intermediate and the minimum increase in the average wave velocity, respectively. The velocity maps confirmed that the grout injection can positively influence the quality of the masonry, since increments in the wave velocity were registered on the entire surface of the samples. However, it is also noticeable that the most significant improvements are quite localized in some regions of the samples and, particularly, close to the points used for the injection and in the lower portion of the specimens.

Diagonal compression test results

Results of the diagonal compression tests are here presented to analyze the efficiency of the adopted strengthening systems in improving the structural performance of stone masonry, in terms of shear capacity, stiffness and failure mode. The results are summarized in Table 4 in terms of peak force P_f, peak shear stress τ_u, masonry tensile strength f_t (evaluated according to Eq. 3) and shear elastic modulus G. Shear stress τ *vs* shear strain γ diagram is presented in Figure 11*a* while in Figure 11*b* an enlargement for

small shear strains (<0.006) is reported.

Considering the result of the unreinforced masonry sample (S_URM), which provided a reference for further comparisons, in the second part of the first ascending branch a growing nonlinear behavior (related to micro-cracks development) can be noticed up to the peak load. From this point, the main crack, aligned along the compressed diagonal, propagated through the mortar joints starting from the center of the panel, showing a failure mode typical for unreinforced masonry samples subject to diagonal compression test (Figure 12*a*). A proper control of the post-peak phase was achieved since the irregular shape of the stones reduced the overall brittleness, by influencing the crack propagation within the mortar and by allowing frictional effects to take place after the onset of cracking.

Concerning samples strengthened by means of grout injection only, the sample S_I reached almost the same peak load of the unreinforced sample, while the peak load for the sample S_I-MA was significantly higher. These results are not consistent with the fact that both the specimens underwent the same strengthening procedure, except from the use of mechanical anchorages. Even if the behavior of the samples can be improved by providing transversal connection between the wall leaves, the great difference observed in the load bearing capacity of the two specimens cannot be associated to the role of the mechanical anchorages only, especially considering an in-plane behavior (Ferretti et al. 2017). By looking at the detail of the cross section of the samples along the main fracture line (Figure 13), it is clearly visible that the two panels were characterized by very different conditions: the grout injection was very effective for the sample S_I-MA (Figure 13*b*), while a great percentage of voids is still visible for the specimen S_I (Figure 13*a*). This is the reason why the sample S_I showed a shear behavior very similar to the one of the unreinforced specimen, especially in terms of peak load and failure mode

(Figure 12*b*). It is not possible to state that the grout injection on the sample S_I was not effective at all, given that a stiffer behavior, with respect to the unreinforced sample, was observed. However, the value of the shear modulus for the sample S_I was lower than the one of the sample S_I-MA, confirming that the grout injection was really efficient, in terms of homogeneity provided to the masonry, only for the latter. Both samples failed with a mechanism similar to that observed for the unreinforced specimen, with cracks along the compressed diagonal. A more widespread state of damage was observed for the sample S_I-MA, with the presence of several cracks. From these observations, it can be stated that analyzing the quality of grout injection is crucial for the study of the improvement given by the adopted strengthening systems.

The shear behavior of samples strengthened by means of FRCMs with symmetric layout is characterized by an initial linear branch, followed by a progressive stiffness decrease, probably corresponding to the cracking of the masonry substrate, up to the peak load, where the first macro-crack appeared on the external surfaces of the samples, involving the mortar matrix. A significant drop in the load bearing capacity was registered after the peak. However, the panels showed a residual strength due to the presence of the reinforcing fibers, able to carry the tensile stresses at large slips and in presence of cracked masonry and to influence the damage propagation within the sample. The failure mode of FRCM strengthened samples was, indeed, characterized by a widespread cracking of the substrate and the matrix (Figure 12*c*). At the end of the tests, both delamination and tensile rupture of some fibers were observed.

The sample which showed the highest increment, both in terms of shear capacity and stiffness, was the sample S_I-MA_S600, strengthened with discontinuous unidirectional steel fiber strips. The first crack appeared in the central portion of the sample, unreinforced, in correspondence of the peak load. Afterwards, it propagated

towards the corners of the sample crossing the reinforcing fiber strips, which resulted damaged at the end of the test, showing the cracking of the matrix and the tensile rupture of few steel fibers (Figure 12*d*). Moreover, in correspondence with high values of horizontal strain, the detachment of the fiber strips extremities was observed. Since the first crack appeared where no reinforcement was placed (discontinuous arrangement of the strips), the increment in the load bearing capacity can be directly associated to the quality of the grout injection, which were verified as to be very efficient by looking at the cross section of the sample after the test, as shown in Figure 14*c*. It can be stated that, in this case, the FRCM strengthening system influenced mainly the post-peak behavior rather than the peak load and it was significantly damaged only in the final part of the test. Moreover, the increment in the shear modulus can also be explained with the fact that grout injection was efficiently performed on the sample. The situation in which the central portion of the panel is not strengthened with FRCMs, as for the chosen arrangement of the unidirectional steel fiber strips, is not the optimal one for the evaluation of the FRCM system improvement but it is anyway worthy of investigation since it corresponds to one of the worst conditions for the retrofitted masonry panel.

The two samples reinforced with the bidirectional basalt grids were characterized by a very similar behavior and reached almost the same peak load, when the macro-cracking of the matrix occurred. By investigating the quality of the grout injection, it was found that they were not fully effective since the internal voids of the samples were not completely filled (Figure 14*a-b*). The failure loads, indeed, were both lower than the peak load of the sample S_I-MA_S600 even if a different trend would be expected since continuous strengthening systems were supposed to be more efficient than the discontinuous one. The peak load was the same for the two samples, irrespective of the amount of fiber reinforcement, because it corresponded to the cracking of the mortar

matrix. As already noticed, the presence of the bidirectional basalt grid influenced mainly the post-peak behavior, determining a more ductile failure mode. Very small differences were registered in this phase, even if one of the samples was reinforced with a double amount of fibers. This can be due to the small bundle spacing of the basalt grid B400, which did not allow the mortar matrix to effectively penetrate within the grid. Thus, a weaker behavior of this strengthening system was observed, with a failure governed by delamination or slipping phenomena rather than by the tensile failure of the fibers, noticed instead for the grid B200. The results of the single-lap shear tests performed for the mechanical characterization of the basalt bidirectional grids are consistent with these observations. Indeed, the bond strength of the grid B400 was significantly lower (58%) than the bond strength of B200. Therefore, a similar improvement of the two FRCM systems could be expected, despite the different density.

The shear behavior of the panel strengthened with an asymmetric layout (S_I-MA_B200-S600) was characterized by a plateau in correspondence of the peak load, which can be associated to the growing effectiveness of the structural repointing after the onset of cracking, with the steel cords gaining force during the crack opening. The values of the peak load and of the shear modulus, significantly lower with respect to the other strengthened samples, were influenced both by the poor-quality of the injection (Figure 14*d*) and by the asymmetry of the reinforcement layout.

The Digital Image Correlation (DIC) technique allowed to obtain strain maps on the entire samples surface during the tests. For sake of comparison, horizontal strain maps for three representative samples are presented, referred to three particular test conditions: i) point *A*, before the peak load, in correspondence of a consistent stiffness decrease (Figure 15); ii) point *B*, in correspondence of the peak load (Figure 16); iii) point *C*, in

correspondence of a horizontal displacement of 2 mm (Figure 17). The chosen points are also represented on the shear stress τ *vs* shear strain γ diagram of Figure 11*b*.

The cracking formation is clearly recognizable (Figure 15*a*-*b*) in the center of the panels, where the maximum horizontal strains were registered, as expected. However, at this point, the crack was not yet visible on the samples surface. For the panel S_I-MA_B400, in particular, the reached deformation values, compatible with the observed stiffness decrease, could be associated to the cracking of the masonry substrate. In accordance with the high value of shear stiffness obtained for the sample S_I-MA_S600 (Figure 15*c*), due to the efficient grout injection, lower values of horizontal strains were registered in the center of this panel.

At the peak load, the crack was significantly open for the sample S_I (Figure 16*a*). Lower deformations were registered for the other two samples, with greater values in the center of the specimens, where the cracking became evident from this point on. The evolution of the crack is shown in Figure 17, where a significant state of damage can be noticed along the compressed diagonal of the samples. The widespread cracking is particularly evident in Figure 17*b*, proving the efficiency of continuous strengthening systems. Referring to Figure 17*c*, it is interesting to observe that lower strain values, with respect to the unreinforced central portion of the sample, were registered in correspondence of the unidirectional steel fiber strips, as expected.

Discussion of results

A comparison between the sonic test results and the failure modes observed from the diagonal compression tests is presented in Figure 18, where the main cracking pattern has been overlapped to the wave velocity maps for the chosen representative samples. By looking also at Figure 15 and Figure 16, a trend can be recognized, with the cracks starting at the center of the panels in correspondence with points characterized by very low local

wave velocities. The cracking propagation towards the corners was influenced by the quality of the specimens as well. Indeed, the fracture lines crossed the portions of the samples where quite low wave velocities were registered. These observations confirm the crucial role played by the grout injection on the overall behavior of the strengthened masonry panels. On the one hand, by increasing the effective resistant cross section, they were able to influence the response of the samples in terms of shear capacity, as already observed. On the other hand, the fact that they did not determine homogenous improvements to the quality of the stone masonry samples influenced the onset of cracking and its following propagation. More in detail, the greater the increase in the local wave velocity given by the injection in the center of the samples, the higher the peak load reached. Indeed, given that the failure in the diagonal compression tests started with the tensile cracking in the center of the samples, the increments given by the injection in terms of local wave velocity were more significative than increments in terms of average wave velocity. This finding can also explain the apparently incoherent result obtained for the sample S_I, which was characterized by a very low value of peak load, despite the consistent increment in the average wave velocity measured from the sonic tests carried out after the strengthening procedure. In fact, a quite low value of the local wave velocity was registered for this sample in correspondence of the central portion of the panel where the diagonal crack started.

Given the influence that the grout injection can have on the test outcomes, a particular attention should be paid during their execution. It is important, indeed, to ensure the effective filling of the voids within the wall leaves. For this purpose, a quantitative control of the amount of the injected mortar should be carried out during this type of activity. In the present experimental campaign, the injection was arrested if a significant increase in the mortar pressure occurred. However, a pressure increase could indicate

either the complete filling of the voids within the sample or the clogging of the hoses used for the injection. In the latter case, the efficiency of the grout injection could be drastically reduced, as observed.

The state of damage of the FRCM strengthened samples at the end of the test was characterized by the presence of multiple fracture lines, not highlighted in Figure 18, involving both the masonry substrate and the matrix. The reinforcing fibers, indeed, were effectively able to transfer the tensile stresses to a wider area and to influence the failure mode of the samples. Considering all the results of the experimental campaign, it can be stated that the adopted strengthening procedures were all efficient in improving the shear behavior of stone masonry samples. In particular, the value of the peak load was influenced mainly by the grout injection, which were not completely effective for all the masonry samples, and, secondly, by the presence of the mortar matrix layers. The reinforcing fiber strips and grids, instead, determined mainly the "ductility" of the failure mode (post-peak behavior). As a confirmation, panels S_I-MA and S_I-MA_S600 provided for the same shear capacity since they had similar effectiveness of grout injection, irrespective of the presence of an external reinforcement; on the contrary, after the onset of cracking, panel S_I-MA showed a more brittle behavior, with the shear capacity rapidly disappearing. The negative slope of the post-peak curve was even larger than that of the unreinforced panel (S_URM), suggesting that injection alone can improve the capacity, but it can also increase the brittleness of the failure.

Analytical formulations

The in-plane shear capacity of a FRCM strengthened masonry panel can be analytically evaluated according to the design formulations proposed in international technical guidelines (ACI 549.4R-13, CNR-DT 215/2018), which are typically based on an additive approach, where the fiber contribution is added to the plain masonry

contribution. The scope of the present Section is to compare experimental results with analytical predictions, evaluated through the formulation proposed by the CNR Italian Guidelines (CNR-DT 215/2018), reported in Equation 6 in terms of shear stresses:

$$\tau_{t,r} = \tau_f + \tau_{t,f} = \tau_f + \frac{n_f \cdot t_{Vf} \cdot l_f \cdot \alpha_t \cdot E_f \cdot \varepsilon_{fd}}{\gamma_{Rd} \cdot A_n} \quad (6)$$

where $\tau_{t,r}$ is the shear strength of the strengthened panel, τ_f is the shear strength of the plain masonry, and $\tau_{t,f}$ is the fiber shear contribution. Moreover, n_f is the number of reinforcing layers, t_{vf} is the fiber equivalent thickness, l_f is the width of the FRCM system measured orthogonally to the shear force, α_t is a coefficient taking into account a reduced tensile strength for fibers subjected to shear, equal to 0.8, E_f is the fiber elastic modulus, ε_{fd} is the design strain of the FRCM system, calculated as 1.5 times the ratio between the bond strength and the modulus E_f to account for an intermediate failure mechanism, γ_{Rd} is a safety factor, considered here equal to 1, and A_n is the net area of the panel cross section. For asymmetric applications, the design strength should be reduced of the 30% at least.

The shear strength predictions are calculated for all the strengthened specimens and reported in Table 4 considering two approaches, differing one from the other in the determination of the plain masonry contribution:

- According to the first approach, corresponding to $\tau_{t,r}$ in Table 4, the masonry shear strength τ_f is considered equal either to the experimental shear strength of the URM sample (S_URM) or to the experimental shear strength of the sample S_I-MA, in which the grout injection was fully effective. The two reported values for $\tau_{t,r}$ correspond to two limit conditions: one in which the injection is not present (or not effective at all) and one in which the injection is correctly performed and fully effective.

- The second approach, corresponding to $\tau_{t,r,NTC}$ in Table 4, is applicable when experimental results on unreinforced masonry are not available; in this case, the shear strength of the plain masonry could be derived from the indications provided by the Italian Building Code and Commentary (NTC 2018), which provides ranges for the values of the average shear strength $\tau_{0,d}$ (in the absence of vertical stresses) of different Italian stone masonry typologies. According to this approach, the shear strength τ_f is computed using the well-known Turnsek-Čačovic's formulation:

$$\tau_f = \frac{1.5 \cdot \tau_{0,d}}{b} \sqrt{1 + \frac{\sigma_0}{1.5 \cdot \tau_{0,d}}}, \quad (7)$$

where the coefficient b is taken equal to 1 (square panels). In the calculations, $\tau_{0,d}$ is considered either the maximum value provided by the Code for the investigated stone masonry typology, equal to 0.074 MPa, or the same value multiplied by an amplification factor, suggested by the Code and equal to 1.5, to account for the presence of the grout injection. Indeed, also in this case, two limit values for $\tau_{t,r,NTC}$ are reported, corresponding to non-effective and effective injection, respectively. To be able to compare the analytical predictions with the experimental results, the compressive stress σ_0 is here considered as the experimental compressive stress component in the test S_URM (non-effective injection) or S_I-MA (effective injection), according to Equation (1).

The value range obtained from the first approach is significantly higher than the value range derived from the second approach. Given that the fiber contribution $\tau_{t,f}$ is the same in both cases, the difference can be attributed to the plain masonry contribution only. In the second approach, the values of the shear strength τ_f are lower than the experimental ones, since they are proposed by the Italian Code for poor-quality masonry. Moreover, the amplification factor proposed by the Italian code to account for grout

injection is significantly lower than the strength increment experimentally observed between the sample S_URM and S_I-MA, equal to 2.5.

Considering the first approach, which gives shear strength predictions closer to the experimental outcomes, it can be observed that the analytical formulation underestimates the experimental results if the grout injection effect is not taken into account but overestimates them in case of effective grout injections. Indeed, the experimental outcomes fall within the range identified for the theoretical shear strength of the strengthened panels ($\tau_{t,r}$). In particular, they are closer to the inferior limits of the interval. This could be considered quite consistent with the fact that: (i) the grout injection was not fully effective for panels reinforced through continuous strengthening systems, and (ii) the layout of the unidirectional fiber strips for the discontinuous strengthening system was not optimal. However, a potential issue should be highlighted concerning the application of the reported analytical formulation. Indeed, the peak load was experimentally observed in correspondence of the cracking of the mortar matrix, which is not taken into account here. At that point, the reinforcing grid has not reached the failure yet, therefore the calculated fiber contribution could be overestimated.

Conclusions

In the present work, an experimental campaign on rubble stone masonry samples strengthened by means of grout injection and Fiber Reinforced Cementitious Matrices (FRMC) was presented. Different strengthening systems were adopted with the aim of comparing their performances in terms of shear capacity and failure mode. Preliminary non-destructive sonic tests were performed to evaluate the masonry quality before and after the strengthening procedure. Then, destructive diagonal compression tests were conducted to analyze the efficiency of the different strengthening systems in improving the shear behavior of rubble stone masonry. The use of analytical formulations for the

prediction of the shear strength of FRCM strengthened masonry panels was also investigated, including the effectiveness of the grout injection.

The results of the sonic tests demonstrated that the grout injection did not always ensure a homogeneous behavior of the strengthened specimens. Indeed, even if average increases in the wave velocity were registered for all the samples, there were some portions of few specimens in which the injection was not completely effective. In these portions, low values of local wave velocity were registered, which, especially if located in the center of the panels (critical areas), influenced the failure load in the diagonal compression test. Typically, the lower the local wave velocity, the lower the peak load reached.

The results of the diagonal compression tests allowed to analyze the effectiveness of both the grout injection and the strengthening systems on the shear behavior of the rubble stone masonry panels. It can be highlighted that all the FRCM strengthened samples were characterized by an increase in the failure load and in the shear stiffness, with respect to the unreinforced masonry specimen, used as reference. As expected, the sample strengthened with an asymmetric layout was characterized by a lower increment with respect to the other reinforced samples. It was found that these increments were mainly associated to the effectiveness of the grout injection and to the presence of the mortar matrix, which cracked in correspondence of the peak load. Once the substrate and the matrix were cracked, the reinforcing fibers, carrying the tensile stresses, influenced the post-peak behavior and the failure mode of the samples, which shifted from the quasi-brittle behavior of the unreinforced sample to more ductile failure modes.

It can be concluded that the efficiency of the grout injection in filling the voids of the samples, providing a greater effective resistant cross section, is crucial for the shear capacity of strengthened masonry panels. Indeed, comparing the results and considering

only the shear strength values, their correct execution seemed to be more important than the choice about the specific FRCM strengthening system to be applied. The fiber typology and layouts influenced the post-peak behavior, as mentioned. In the experimental campaign, large differences were not observed in the post-peak phase of the strengthened specimens even if it could be expected that the application of a continuous strengthening system instead of a discontinuous one could determine a better stress redistribution, a more widespread cracking of the specimens and, as a consequence, a more ductile behavior. To better capture the improvement given by the FRCM strengthening systems in terms of shear strength for this type of masonry, the study of the uncoupled effect of grout injection and FRCMs on the shear behavior of rubble stone masonry could be the object of future research.

Acknowledgments

The financial and technical support of Kerakoll Spa, Sassuolo (MO) Italy, and the financial support of the Italian Department of Civil Protection (ReLUIS 2019 Grant – Innovative Materials) are gratefully acknowledged. Mr. Diiterihs Erra, Mr. Michele Esposito (Technical staff at CIRI Buildings & Construction) and the master student Ylenia Leonardi are gratefully acknowledged for their work during the setup of the tests.

Conflict of interest

On behalf of all authors, the corresponding author states that there is no conflict of interest.

References

ACI 549.4R-13. Guide to design and construction of externally bonded Fabric-Reinforced Cementitious Matrix (FRCM) systems for repair and strengthening concrete and masonry structures. 2013.

ASTM International. 2015. ASTM E519/E519M-15 Standard Test Method for Diagonal Tension (Shear) in Masonry Assemblages. West Conshohocken, PA; ASTM International. doi: https://doi.org/10.1520/E0519_E0519M-15.

Augusti, G., M. Ciampoli, and P. Giovenale. 2001. Seismic vulnerability of monumental buildings. *Structural Safety* (23): 253–274.

Babaeidarabad, S., F. De Caso, and A. Nanni. 2014. URM walls strengthened with fabric-reinforced cementitious matrix composite subjected to diagonal compression, *Journal of Composites for Construction* (18): 04013045. doi:10.1061/(ASCE)CC.1943-5614.0000441.

Bellini, A., M. Bovo, and C. Mazzotti. 2019. Experimental and numerical evaluation of fiber-matrix interface behavior of different FRCM systems. *Composites Part B Engineering* (161): 411–426. doi:10.1016/j.compositesb.2018.12.115.

Bellini, A., S.-K. Shahreza, and C. Mazzotti. 2019. Cyclic bond behavior of FRCM composites applied on masonry substrate. *Composites Part B Engineering* (169): 189–199. doi:10.1016/j.compositesb.2019.04.009.

Binda, L. 1995. Role of a RILEM Commitee: calibration of proposed test methods. In *Proceedings of the Joint International Workshop proposed by RILEM TC 127-MS and CIB W23*, 1-24. Padova, Italy.

Binda, L., C. Modena, G. Baronio, and S. Abbaneo. 1997. Repair and investigation techniques for stone masonry walls. *Construction and Building Materials* (11): 133–142. doi:10.1016/S0950-0618(97)00031-7.

Binda, L., A. Saisi, and C. Tiraboschi. 2000. Investigation procedures for the diagnosis of historic masonries. *Construction and Building Materials* (14): 199–233. doi:10.1016/S0950-0618(00)00018-0.

Binda, L., A. Saisi, and C. Tiraboschi. 2001. Application of sonic tests to the diagnosis of damaged and repaired structures. *NDT & E International* (34): 123–138. doi:10.1016/S0963-8695(00)00037-2.

Binda, L., G. Cardani, A. Saisi, and C. Groot. 2005. A classification of structures and masonries for the adequate choice of repair. *International RILEM Workshop on Repair Mortars for Historic Masonry*, RILEM publications – Pro 67: 20-34.

Borri, A., G. Castori, M. Corradi, and E. Speranzini. 2011. Shear behavior of unreinforced and reinforced masonry panels subjected to in situ diagonal compression tests. *Construction and Building Materials* (25): 4403–4414. doi:10.1016/j.conbuildmat.2011.01.009.

Caggegi, C., F.-G. Carozzi, S. De Santis, F. Fabbrocino, F. Focacci, Ł. Hojdys, E. Lanoye, and L. Zuccarino. 2017. Experimental analysis on tensile and bond properties of PBO and aramid fabric reinforced cementitious matrix for strengthening masonry structures. *Composites Part B Engineering* (127):175–195. doi:10.1016/j.compositesb.2017.05.048.

Calderini, C., S. Cattari, and S. Lagomarsino. 2010. The use of the diagonal compression test to identify the shear mechanical parameters of masonry. *Construction and Building Materials* (24): 677–685. doi:10.1016/j.conbuildmat.2009.11.001.

Carozzi, F.-G., A. Bellini, T. D'Antino, G. de Felice, F. Focacci, Ł. Hojdys, L. Laghi, E. Lanoye, F. Micelli, M. Panizza, et al. 2017. Experimental investigation of tensile and bond properties of Carbon-FRCM composites for strengthening masonry elements. *Composites Part B Engineering* (128):100–119. doi:10.1016/j.compositesb.2017.06.018.

Ceci, A.-M, A. Contento, L. Fanale, D. Galeota, V. Gattulli, M. Lepidi, and F. Potenza. 2010. Structural performance of the historic and modern buildings of the University of L'Aquila during the seismic events of April 2009. *Engineering Structures* (32): 1899–1924. doi:10.1016/j.engstruct.2009.12.023.

CNR-DT 215/2018, Guide for the design, execution and control of strengthening interventions by means of fiber reinforced composite materials with inorganic matrices (in Italian), National Research Council, 2018.

D'Ayala, D., and E. Speranza. 2003. Definition of collapse mechanisms and seismic vulnerability of historic masonry buildings. *Earthquake Spectra* (19): 479–509. doi:10.1193/1.1599896.

de Felice, G., M.-A. Aiello, A. Bellini, F. Ceroni, S. De Santis, E. Garbin, M. Leone, G.-P. Lignola, M. Malena, C. Mazzotti, et al. 2016. Experimental characterization of composite-to-brick masonry shear bond. *Materials and Structures* (49): 2581–96. doi:10.1617/s11527-015-0669-4.

de Felice, G., M.-A. Aiello, C. Caggegi, F. Ceroni, S. De Santis, E. Garbin, N. Gattesco, Ł. Hojdys, P. Krajewski, A. Kwiecień, et al. 2018. Recommendation of RILEM Technical Committee 250-CSM: Test method for Textile Reinforced Mortar to substrate bond characterization. *Materials and Structures* (51): 95. doi:10.1617/s11527-018-1216-x.

EN 1015 (European Norms). 2006. EN 1015-11:1999/A1:2006 Methods of test for mortar for masonry - Part 11: Determination of flexural and compressive strength of hardened mortar.

Faella, C., E. Martinelli, E. Nigro, and S. Paciello. 2010. Shear capacity of masonry walls externally strengthened by a cement-based composite material: An experimental campaign. *Construction and Building Materials* (24): 84–93. doi:10.1016/j.conbuildmat.2009.08.019.

Feo, L., R. Luciano, G. Misseri, and L. Rovero. 2016. Irregular stone masonries: Analysis and strengthening with glass fibre reinforced composites. *Composites Part B Engineering* (92): 84–93. doi:10.1016/j.compositesb.2016.02.038.

Ferretti, F., A.-R. Tilocca, B. Ferracuti, and C. Mazzotti. 2015. In situ diagonal compression tests on masonry panels strengthened by FRP and FRCM. In *12th International Symposium on Fiber Reinforced Polymers for Reinforced Concrete Structures (FRPRCS-12) & 5th Asia-Pacific Conference on Fiber Reinforced Polymers in Structures (APFIS-2015) Joint Conference*. Nanjing, China.

Ferretti, F., B. Ferracuti, A. Incerti, and C. Mazzotti. 2016. Diagonal compression tests on masonry panels strengthened by FRP and FRCM. In *Structural Analysis of Historical Constructions*, ed. K. Van Balen and E. Verstrynge, 1069–76. Leuven, Belgium: CRC Press/Balkema. doi:10.1201/9781315616995-159.

Ferretti, F., A. Incerti, B. Ferracuti, and C. Mazzotti. 2017. FRCM strengthened masonry panels: the role of mechanical anchorages and symmetric layouts. *Key Engineering Materials* (747): 334–341. doi:10.4028/www.scientific.net/KEM.747.334.

Frocht, M. 1931. Recent advances in photoelasticity, *ASME Trans.* (55): 135–153.

Gattesco, N., C. Amadio, and C. Bedon. 2015. Experimental and numerical study on the shear behavior of stone masonry walls strengthened with GFRP reinforced mortar coating and steel-cord reinforced repointing. *Engineering Structures* (90): 143–157. doi:10.1016/j.engstruct.2015.02.024.

Guerreiro, J., J. Proença, J.G. Ferreira, and A. Gago. 2018. Experimental characterization of in-plane behavior of old masonry walls strengthened through the addition of CFRP reinforced render. *Composites Part B Engineering* (148): 14–26. doi:10.1016/j.compositesb.2018.04.045.

Incerti, A., A. Vasiliu, B. Ferracuti, and C. Mazzotti. 2015. Uniaxial compressive tests on masonry columns confined by FRP and FRCM. In *12th International Symposium on Fiber Reinforced Polymers for Reinforced Concrete Structures (FRPRCS-12) & 5th Asia-Pacific Conference on Fiber Reinforced Polymers in Structures (APFIS-2015) Joint Conference*. Nanjing, China.

Incerti, A., M. Santandrea, C. Carloni, and C. Mazzotti. 2017. Destructive in situ tests on masonry arches strengthened with FRCM composite materials. *Key Engineering Materials* (747): 567–573. doi:10.4028/www.scientific.net/KEM.747.567.

Incerti, A., A.-R. Tilocca, F. Ferretti, and C. Mazzotti. 2019. Influence of masonry texture on the shear strength of FRCM reinforced panels. In *Structural Analysis of Historical Constructions*, ed. R. Aguilar, D. Torrealva, S. Moreira, M.-A. Pando and L.-F. Ramos. RILEM Bookseries (18): 1623-21. Springer, Cham. doi:10.1007/978-3-319-99441-3_174.

Incerti, A., F. Ferretti, and C. Mazzotti. 2019. FRCM strengthening systems efficiency on the shear behavior of pre-damaged masonry panels: an experimental study. *Journal of Building Pathology and Rehabilitation* (4): 1-13. doi: 10.1007/s41024-019-0053-9.

Indirli, M., L.-A. S. Kouris, A. Formisano, R.-P. Borg, and F.-M. Mazzolani. 2013. Seismic damage assessment of unreinforced masonry structures after the Abruzzo 2009 Earthquake: the case study of the historical centers of L'Aquila and Castelvecchio Subequo. *International Journal of Architectural Heritage* (7): 536–578. doi:10.1080/15583058.2011.654050.

Italian Building Code (in Italian), Ministry of Infrastructure and Transport, D.M. 17 January 2018.

Italian Building Code Commentary (in italian), Ministry of Infrastructure and Transport, D.M. 21 January 2019.

Jorne, F., F.-M.-A. Henriques, and L.-G. Baltazar. 2014. Evaluation of consolidation of grout injection with ultrasonic tomography. *Construction and Building Materials* (66): 494–506. doi:10.1016/j.conbuildmat.2014.05.095.

Leone, M., M.-A. Aiello, A. Balsamo, F.-G. Carozzi, F. Ceroni, M. Corradi, M. Gams, E. Garbin, N. Gattesco, P. Krajewski, et al. 2017. Glass fabric reinforced cementitious matrix: Tensile properties and bond performance on masonry substrate. *Composites Part B Engineering* (127): 196–214. doi:10.1016/j.compositesb.2017.06.028.

Lignola, G.-P., C. Caggegi, F. Ceroni, S. De Santis, P. Krajewski, P.-B. Lourenço, M. Morganti, C. Papanicolaou, C. Pellegrino, A. Prota, et al. 2017. Performance assessment of basalt FRCM for retrofit applications on masonry. *Composites Part B Engineering* (128): 1–18. doi:10.1016/j.compositesb.2017.05.003.

Luso, E., and P.-B. Lourenço. 2016. Experimental characterization of commercial lime based grouts for stone masonry consolidation. *Construction and Building Materials* (102): 216–225. doi:10.1016/j.conbuildmat.2015.10.096.

Miltiadou-fezans, A., E. Vintzileou, E. Papadopoulou, and A. Kalagri. 2006. Mechanical properties of three-leaf stone masonry after grouting. In *Structural Analysis of Historical Constructions*, eds. P.-B. Lourenço, P. Roca, and C. Modena: 791–798. New Delhi, India.

Miranda, L., J. Milosevic, and R. Bento. 2017. Cyclic behavior of stone masonry walls strengthened by grout injection. *Materials and Structures* (50): 47. doi:10.1617/s11527-016-0911-8.

Papanicolaou, C., T. Triantafillou, and M. Lekka. 2011. Externally bonded grids as strengthening and seismic retrofitting materials of masonry panels. *Construction and Building Materials* (25): 504–514. doi:10.1016/j.conbuildmat.2010.07.018.

Parisi, F., I. Iovinella, A. Balsamo, N. Augenti, and A. Prota. 2013. In-plane behavior of tuff masonry strengthened with inorganic matrix–grid composites. *Composites Part B Engineering* (45): 1657–66. doi:10.1016/j.compositesb.2012.09.068.

Penna, A. Seismic assessment of existing and strengthened stone-masonry buildings: critical issues and possible strategies. 2015. *Bulletin of Earthquake Engineering* (13): 1051-71. doi:10.1007/s10518-014-9659-0.

RILEM TC – LUMB6. 1991. Diagonal Tensile Strength Tests of Small Wall Specimens.

Schuller, M., M. Berra, R. Atkinson, and L. Binda. 1997. Acoustic tomography for evaluation of unreinforced masonry. *Construction and Building Materials* 11: 199–204. doi:10.1016/S0950-0618(97)00038-X.

Silva, B., M. Dalla Benetta, F. da Porto, and C. Modena. 2014. Experimental assessment of in-plane behavior of three-leaf stone masonry walls. *Construction and Building Materials* (53): 149–161. doi:10.1016/j.conbuildmat.2013.11.084.

Valluzzi, M.-R., E. Cescatti, G. Cardani, L. Cantini, L. Zanzi, C. Colla, and F. Casarin. 2018. Calibration of sonic pulse velocity tests for detection of variable conditions in masonry walls. *Construction and Building Materials* (192) 272–286. doi:10.1016/j.conbuildmat.2018.10.073.

Vintzileou, E.-N. 2007. Grouting of three-leaf masonry: experimental results and prediction of mechanical properties. *Evoluzione nella sperimentazione per le costruzioni*: 171–190.

Vintzileou, E.-N, C. Mouzakis, C.-E. Adami, and L. Karapitta. 2015. Seismic behavior of three-leaf stone masonry buildings before and after interventions: Shaking table tests on a two-storey masonry model. *Bulletin of Earthquake Engineering* (13): 3107–33. doi:10.1007/s10518-015-9746-x.

Yokel, F.-Y., and S.-G. Fattal. 1976. A Failure hypothesis for masonry shearwalls. *Journal of Structural Divisions - ASCE* (102): 515–532.

List of tables

Table 1. Characteristics of the tested stone masonry samples.

Table 2. Mechanical properties of the mortars.

Table 3. Mechanical properties of the reinforcing fiber strips and grids.

Table 4. Diagonal compression test results.

List of figures

Figure 1. Stone masonry wall.

Figure 2. Layout of the adopted strengthening systems: (a) sample S_I; (b) sample S_I-MA; (c) sample S_I-MA_S600; (d) samples S_I-MA_B200 and S_I-MA_B400; (e-f) sample S_I-MA_B200-S600.

Figure 3. Reinforcing procedure: (a) drilling of the holes; (b) first mortar matrix layer in case of continuous reinforcement; (c) positioning of the bidirectional grid; (d-e) mechanical anchorages; (f) second mortar matrix layer.

Figure 4. Reinforcing procedure for the sample S_I-MA_B200-S600, Reticolatus technique.

Figure 5. Sonic tests: (a) testing grid over the lateral surface of the samples; (b) test instrumentation.

Figure 6. Diagonal compression test setup.

Figure 7. Sonic test results: average wave velocities.

Figure 8. Sonic wave velocity maps on the sample S_I-MA_S600: (a) pre-strengthening, (b) post-strengthening.

Figure 9. Sonic wave velocity maps on the sample S_I: (a) pre-strengthening, (b) post-strengthening.

Figure 10. Sonic wave velocity maps on the sample S_I-MA_B400: (a) pre-strengthening, (b) post-strengthening.

Figure 11. Diagonal compression test results: shear stress τ vs shear strain γ diagram.

Figure 12. Failure modes: (a) S_URM; (b) S_I; (c) S_I-MA_B400; (d) S_I-MA_S600.

Figure 13. Detail of the cross section of the samples after the tests: (a) sample S_I; (b) sample S_I-MA.

Figure 14. Detail of the cross section of the samples after the tests: (a) sample S_I-MA_B200; (b) sample S_I-MA_B400, (c) sample S_I-MA_S600, (d) sample S_I-MA_B200-S600.

Figure 15. Horizontal strain maps – pre-peak (point A): (a) S_I; (b) S_I-MA_B400; (c) S_I-MA_S600.

Figure 16. Horizontal strain maps – peak load (point B): (a) S_I; (b) S_I-MA_B400; (c) S_I-MA_S600.

Figure 17. Horizontal strain maps – post-peak (point C): (a) S_I; (b) S_I-MA_B400; (c) S_I-MA_S600.

Figure 18. Comparison between sonic test results and failure mode of the diagonal compression test: (a) S_I; (b) S_I-MA_B400; (c) S_I-MA_S600.

Sample Code	Grout Injection	FRCM system characteristics*	Matrix Type	Fiber Type	Mechanical Anchorages
S_URM	-	-	-	-	-
S_I	NHL mortar	-	-	-	No
S_I-MA	NHL mortar	-	-	-	Yes
S_I-MA_B200	NHL mortar	SL, C	NHL mortar	Basalt grid	Yes
S_I-MA_B400	NHL mortar	SL, C	NHL mortar	Basalt grid	Yes
S_I-MA_S600	NHL mortar	SL, D	NHL mortar	Steel fibers	Yes
S_I-MA_B200-S600	NHL mortar	AL, C+D	NHL mortar	Basalt grid Steel fibers	Yes

* SL: symmetric layout, AL: asymmetric layout, C: continuous, D: discontinuous.

Table 1. Characteristics of the tested stone masonry samples.

Mortar	$f_{m,c}$ (MPa)	CoV (%)	$f_{m,fl}$ (MPa)	CoV (%)	E_m (MPa)	CoV (%)
NHL1	4.8	12.5	1.5	15.1	4586	17.3
NHL2	19.6	3.4	4.7	13.9	9500*	-
NHL3	12.6	9.5	2.9	22.6	9100	13.8

*given by the producer.

Table 2. Mechanical properties of the mortars.

Code	Fiber type	Density (g/m^2)	Bundle spacing (mm)	t_{Vf} (mm)	$f_{f,t}$ (MPa)	ε_u (%)	E_f (GPa)	$f_{f,b}$ (MPa)
B200	Bidirectional basalt grid	200	17	0.032	1160	2.2	76.1	1058
B400	Bidirectional basalt grid	400	8	0.064	963	1.1	66.2	616
S600	Unidirectional steel fiber strips	600	-	0.084	2857	1.7	200.9	2688

Table 3. Mechanical properties of the reinforcing fiber strips and grids.

Sample	P_f (kN)	τ_u (MPa)	f_t (MPa)	G (MPa)	$\tau_{t,r}$ (MPa)	$\tau_{t,r,NTC}$ (MPa)
S_URM	122.7	0.39	0.19	728.6	-	
S_I	123.4	0.39	0.19	1988.9	-	
S_I-MA	301.1	0.96	0.46	3059.8	-	
S_I-MA_B200	264.1	0.84	0.40	3369.1	0.65 – 1.22	0.45 – 0.60
S_I-MA_B400	264.9	0.84	0.40	2704.9	0.69 – 1.26	0.49 – 0.64
S_I-MA_S600	298.7	0.95	0.45	4655.5	0.88 – 1.45	0.68 – 0.83
S_I-MA_B200-S600	181.6	0.58	0.28	2440.4	0.48 – 1.05	0.28 – 0.43

Table 4. Diagonal compression test results.

Figure 1. Stone masonry wall.

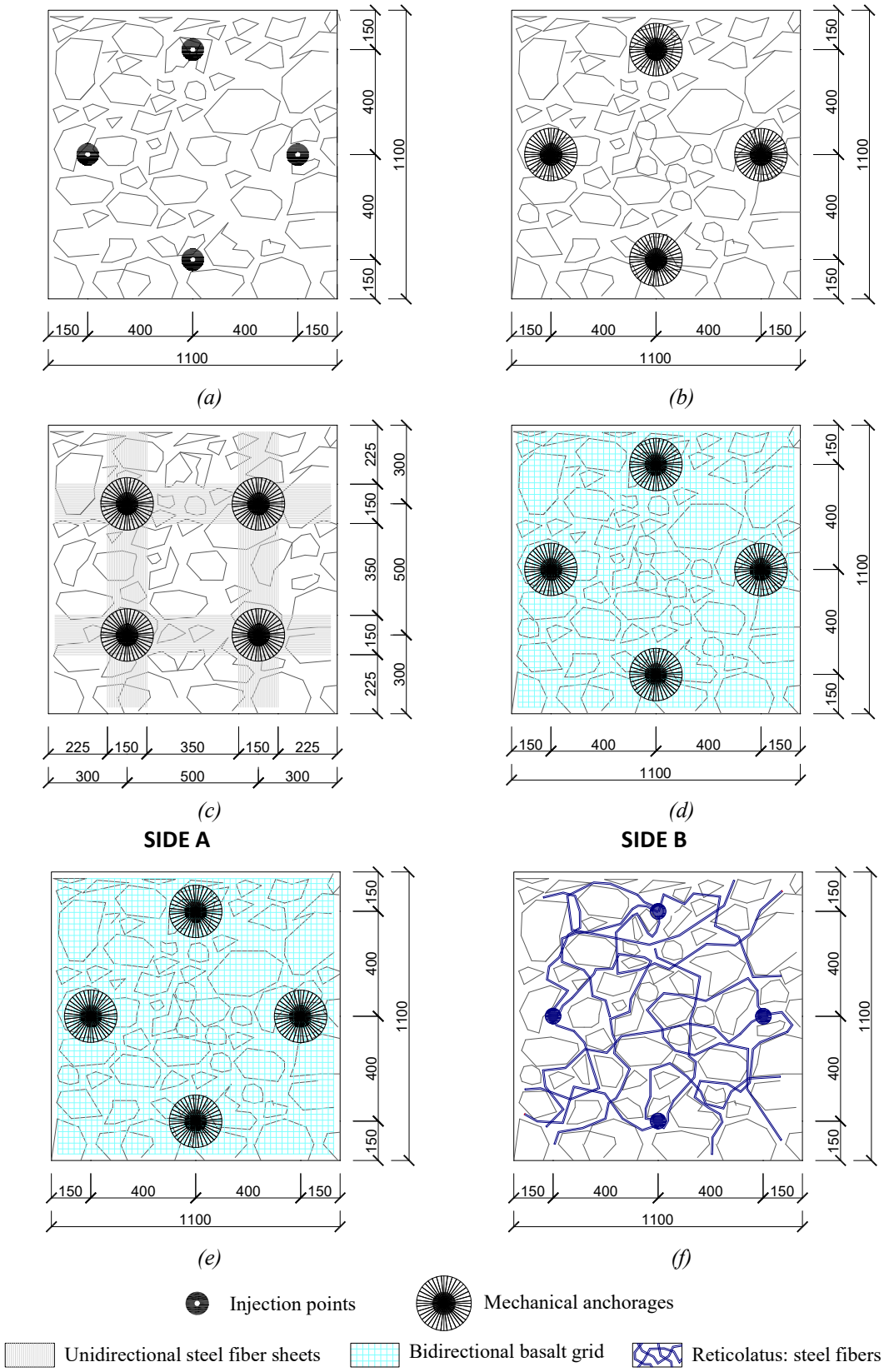

Figure 2. Layout of the adopted strengthening systems: (a) sample S_I; (b) sample S_I-MA; (c) sample S_I-MA_S600; (d) samples S_I-MA_B200 and S_I-MA_B400; (e-f) sample S_I-MA_B200-S600.

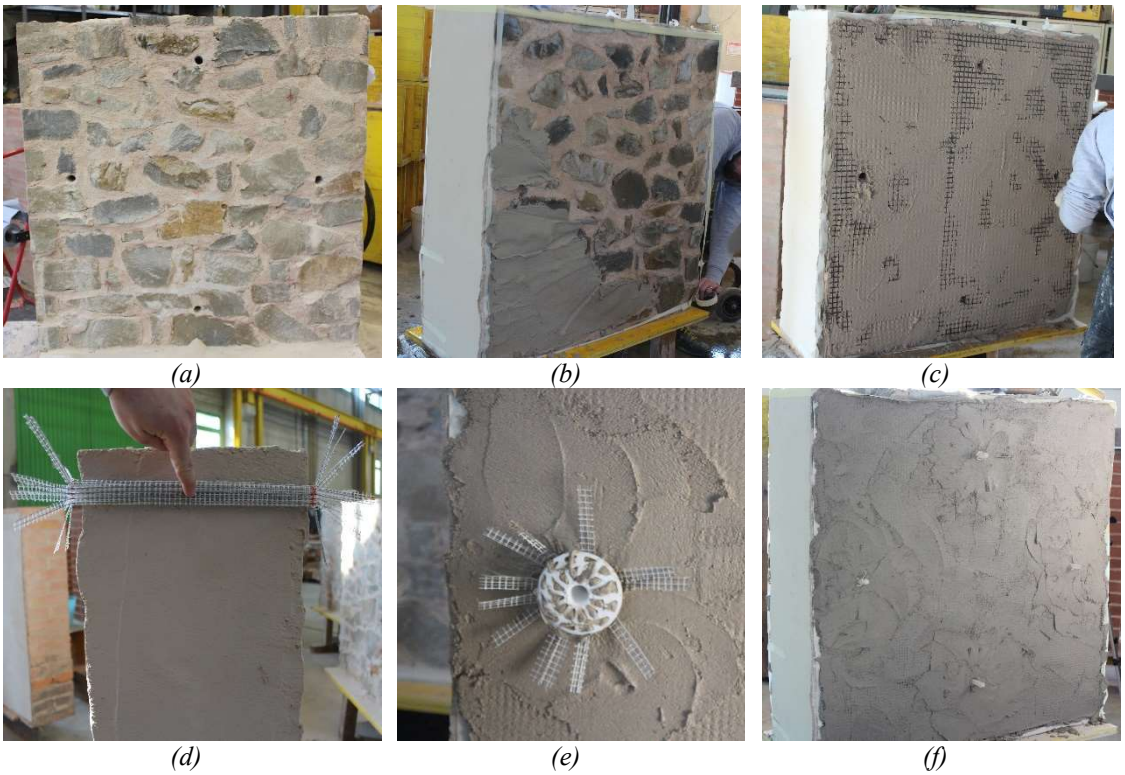

Figure 3. Reinforcing procedure: (a) drilling of the holes; (b) first mortar matrix layer in case of continuous reinforcement; (c) positioning of the bidirectional grid; (d-e) mechanical anchorages; (f) second mortar matrix layer.

Figure 4. Reinforcing procedure for the sample S_I-MA_B200-S600, *Reticolatus* technique.

(a) *(b)*

Figure 5. Sonic tests: (a) testing grid over the lateral surface of the samples; (b) test instrumentation.

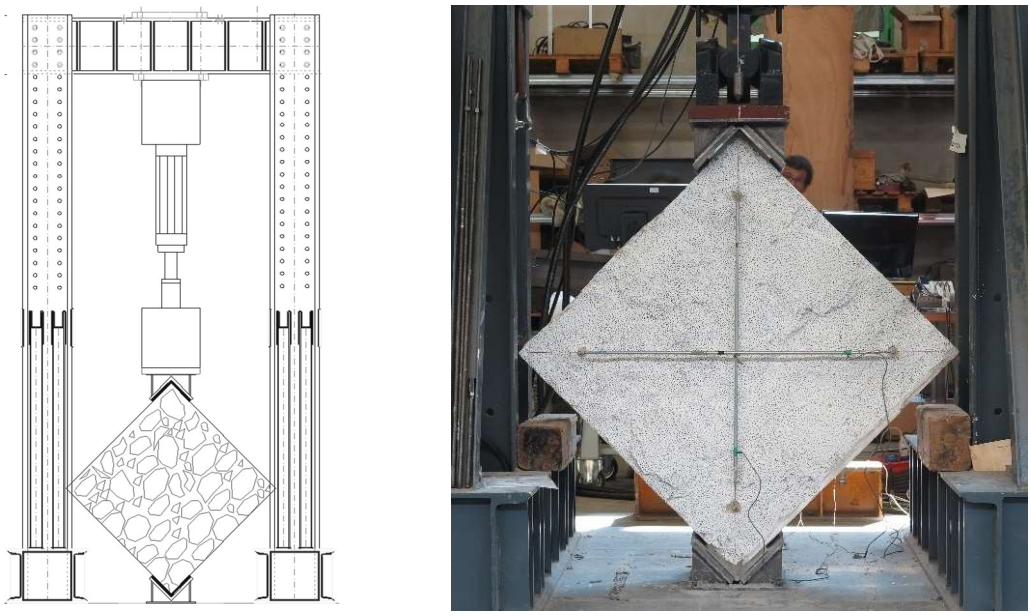

Figure 6. Diagonal compression test setup.

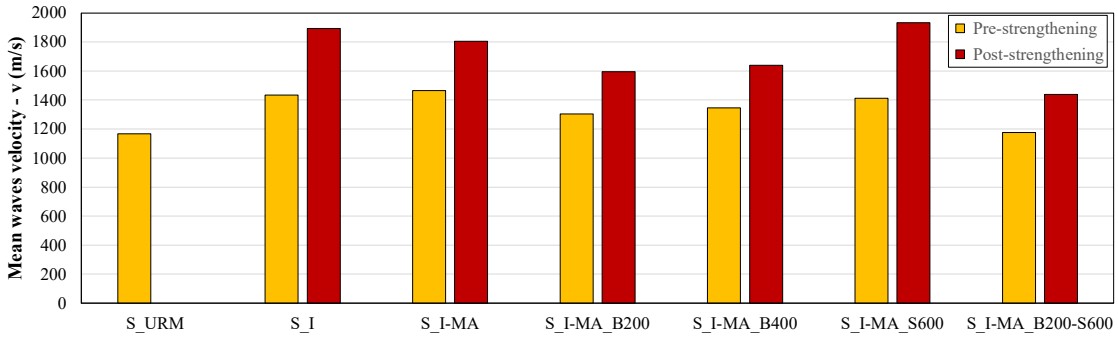

Figure 7. Sonic test results: average wave velocities.

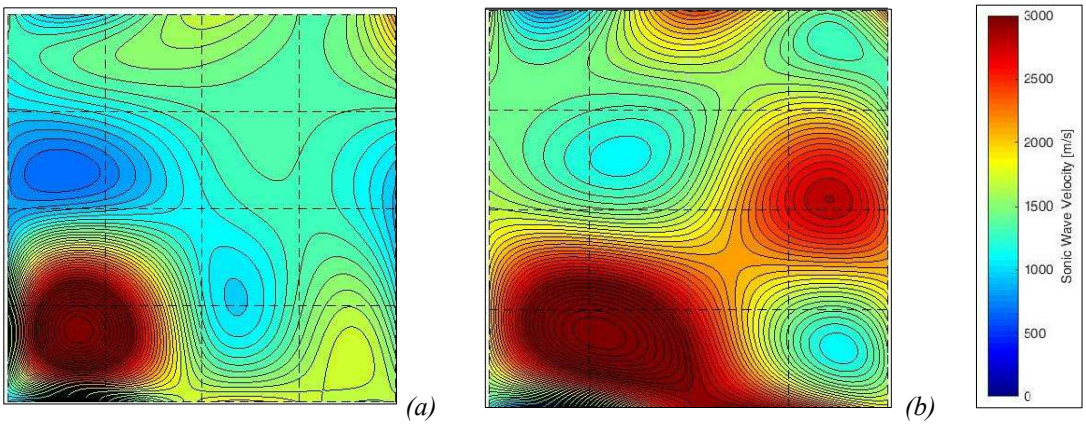

Figure 8. Sonic wave velocity maps on the sample S_I-MA_S600: (a) pre-strengthening, (b) post-strengthening.

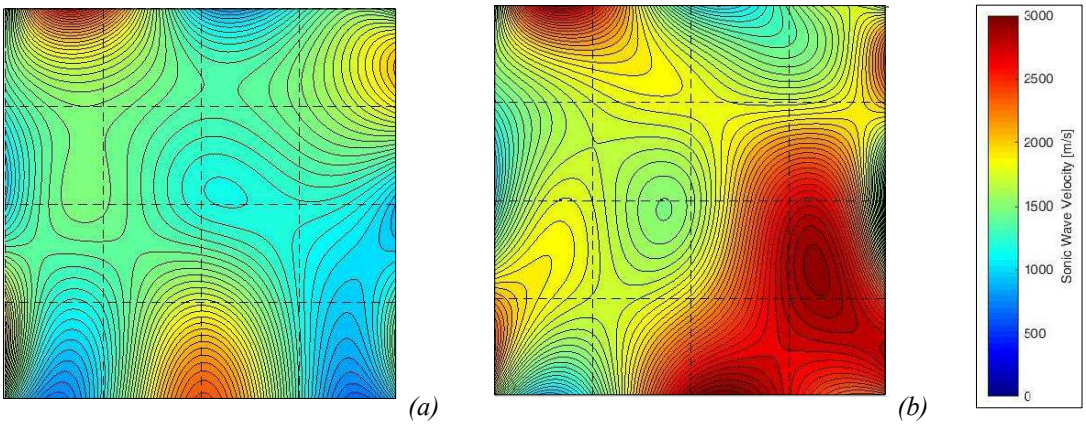

(a) *(b)*

Figure 9. Sonic wave velocity maps on the sample S_I: (a) pre-strengthening, (b) post-strengthening.

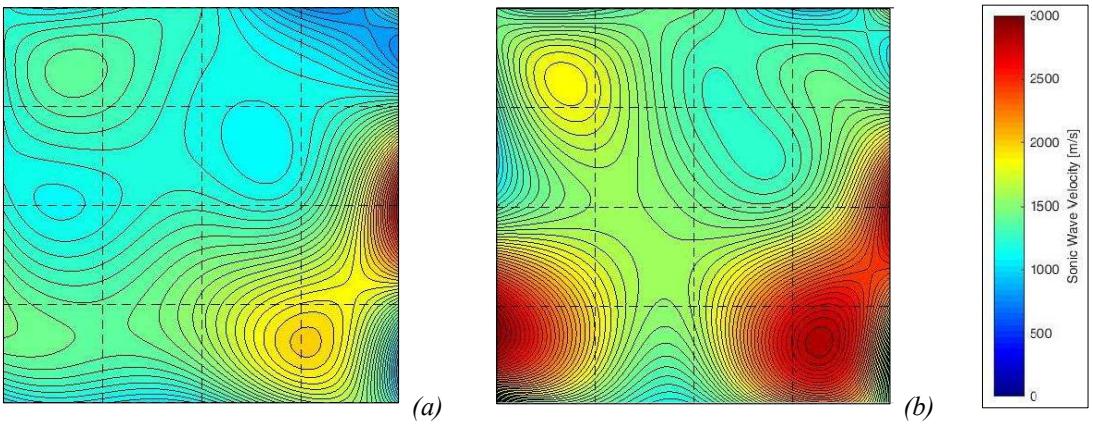

Figure 10. Sonic wave velocity maps on the sample S_I-MA_B400: (a) pre-strengthening, (b) post-strengthening.

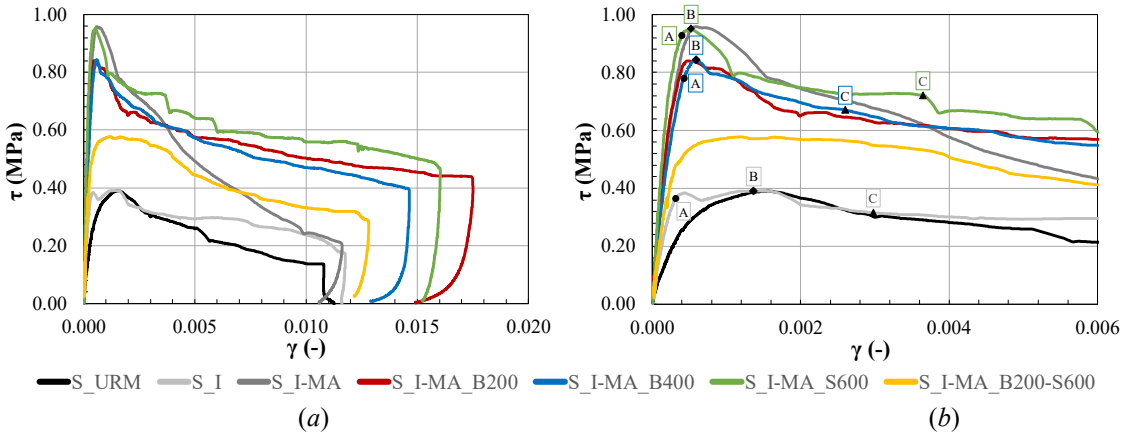

(*a*) (*b*)

Figure 11. Diagonal compression test results: shear stress τ vs shear strain γ diagram.

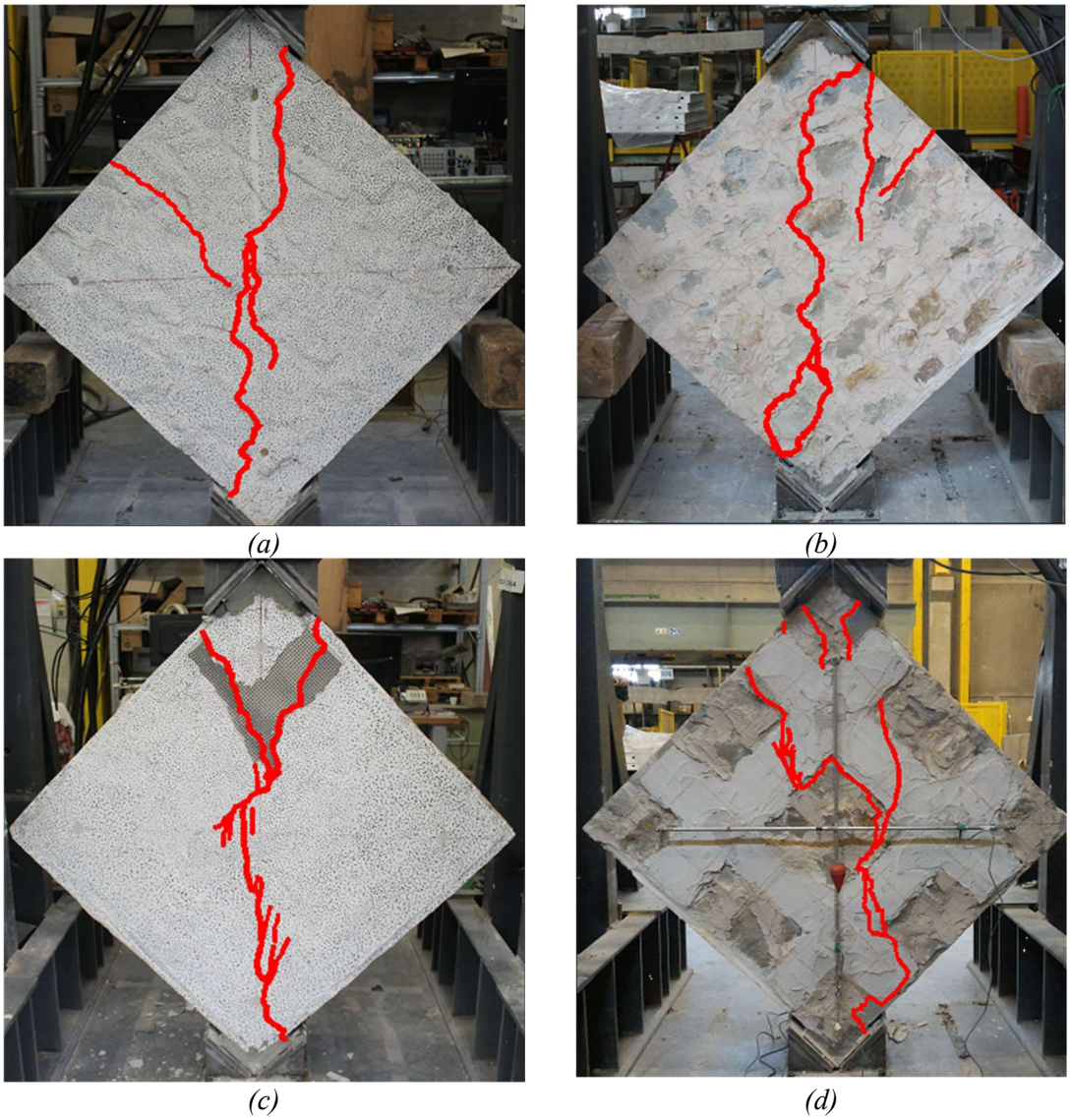

Figure 12. Failure modes: (a) S_URM; (b) S_I; (c) S_I-MA_B400; (d) S_I-MA_S600.

(a) *(b)*

Figure 13. Detail of the cross section of the samples after the tests: (a) sample S_I; (b) sample S_I-MA.

(a) *(b)* *(c)* *(d)*

Figure 14. Detail of the cross section of the samples after the tests: (a) sample S_I-MA_B200; (b) sample S_I-MA_B400, (c) sample S_I-MA_S600, (d) sample S_I-MA_B200-S600.

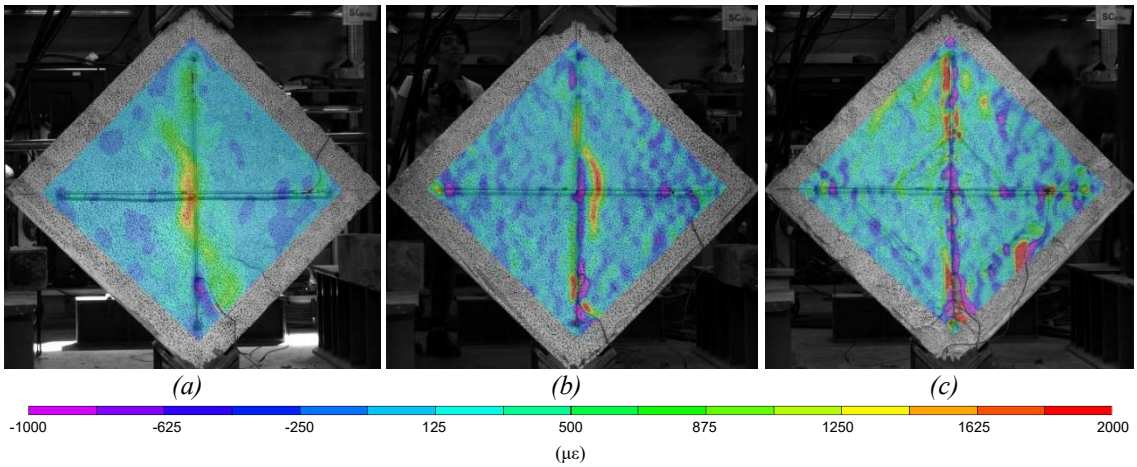

Figure 15. Horizontal strain maps – pre-peak (point A): (a) S_I; (b) S_I-MA_B400; (c) S_I-MA_S600.

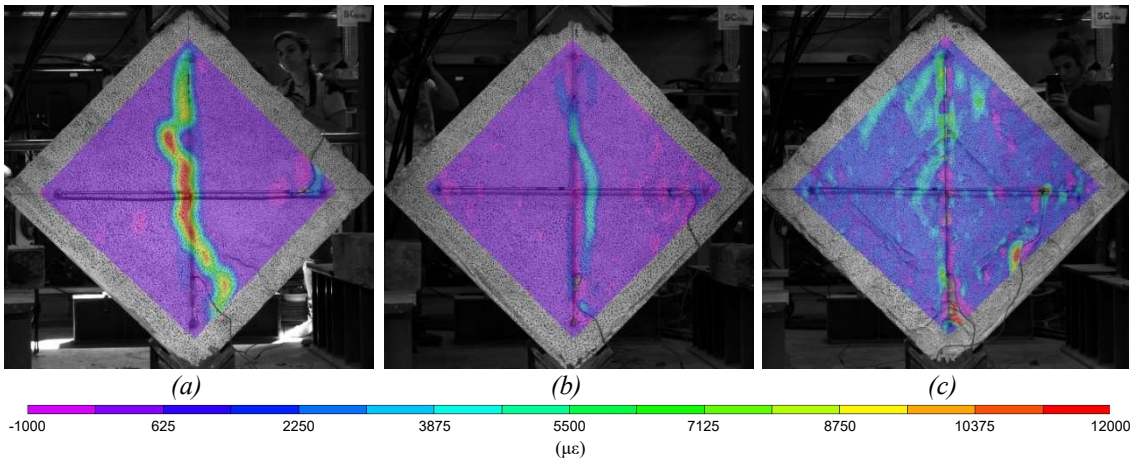

Figure 16. Horizontal strain maps – peak load (point B): (a) S_I; (b) S_I-MA_B400; (c) S_I-MA_S600.

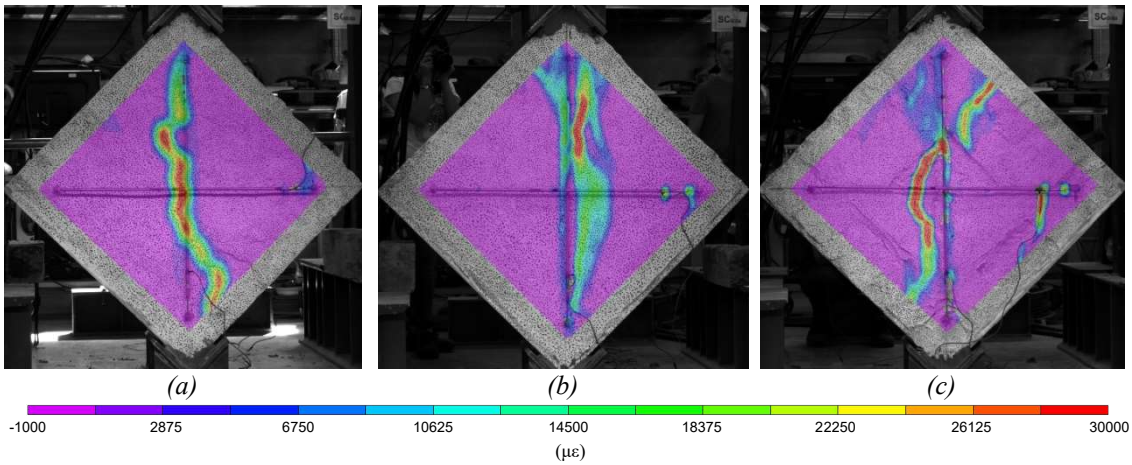

Figure 17. Horizontal strain maps – post-peak (point C): (a) S_I; (b) S_I-MA_B400; (c) S_I-MA_S600.

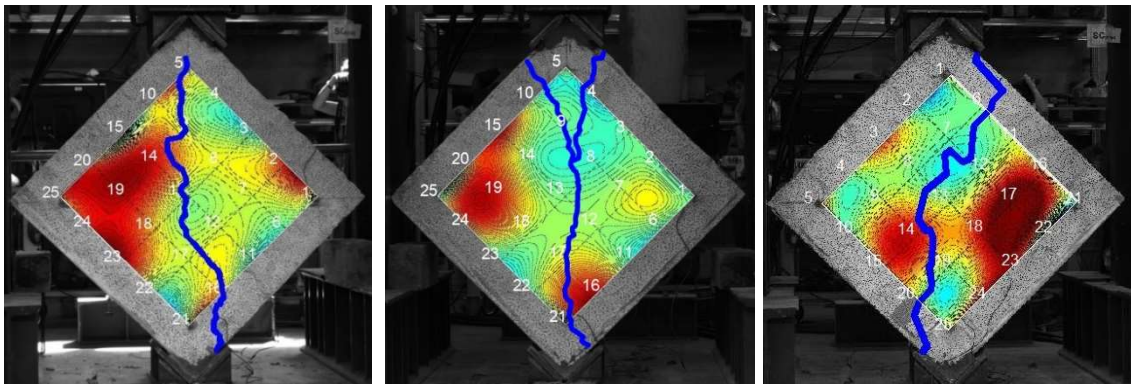

(a) *(b)* *(c)*

Figure 18. Comparison between sonic test results and failure mode of the diagonal compression test: (a) S_I; (b) S_I-MA_B400; (c) S_I-MA_S600.